Thermodynamics of Linear Carbon Chains

Nathalia L. Costa, Keshav Sharma, Yoong Ahm Kim, Go Bong Choi, Morinobu Endo, Newton M. Barbosa Neto, Alexandre R. Paschoal, and Paulo T. Araujo

Phys. Rev. Lett. **126**, 125901 — Published 26 March 2021

DOI: 10.1103/PhysRevLett.126.125901

Thermodynamics of Linear Carbon Chains

Nathalia L. Costa[1,†], Keshav Sharma[2,†], Yoong Ahm Kim[3], Go Bong Choi[3], Morinobu Endo[4], Newton M. Barbosa Neto[5,*], Alexandre R. Paschoal[1,*] and Paulo T. Araujo[2,*]

1 Department of Physics, Federal University of Ceara, 60455-760 Fortaleza, Ceara, Brazil.

2 Department of Physics and Astronomy, University of Alabama, Tuscaloosa, Alabama 35487, USA.

3 Department of Polymer Engineering, School of Polymer Science and Engineering, and Alan G. MacDiarmid Energy Research Institute, Chonnam National University, 77 Yongbong-ro, Buk-gu, Gwangju, 61186, Republic of Korea.

4 Faculty of Engineering, Shinshu University, 4-17-1 Wakasato, Nagano-shi 380-8553, Japan.

5 Institute of Natural Sciences, Graduate Program in Physics, Federal University of Para, 66075-110 Belem, PA, Brazil.

† These authors contributed equally to this work.

* Corresponding authors: paschoal@fisica.ufc.br, barbosaneto@ufpa.br and ptaraujo@ua.edu

Linear carbon chains (LCCs) are one dimensional materials with unique properties, including high Debye's temperatures and restrict selection rules for phonon interactions. Consequently, their Raman C-band frequency's temperature dependence is a probe to their thermal properties, which are well described within the Debye's formalism even at room temperatures. Therefore, with basis on a semi-empirical approach we show how to use the C-band to evaluate the LCCs' internal energy, heat capacity, coefficient of thermal expansion, thermal strain and Grüneisen parameter, providing universal relations for these quantities in terms of the number of carbons atoms and the temperature.

One dimensional (1D) linear carbon chains (LCCs) are one of the simplest materials presenting properties associated to both molecules and solids [1-8], making them ideal for many electronic [9-13], mechanical [14,15] and thermal applications [2,16]. They exhibit sp hybridization and can be either semiconducting, known as polyynes with alternate single and triple bonds ($\cdots -\mathrm{C} \equiv \mathrm{C} - \mathrm{C} \equiv \mathrm{C} - \cdots$), or metallic, also known as cumulenes ($\cdots \mathrm{C} = \mathrm{C} = \mathrm{C} = \mathrm{C} = \cdots$) [8,12]. Historically, host-free LCCs have posed interesting questions regarding their stability [6,17,18] but recently, single-wall (SW), double-wall (DW), and multi-wall (MW) carbon nanotubes (CNT) are considered ideal environments for fabricating stable LCCs with up to 6000 C-atoms [1,5,9,11,15]. The polyynic structure is often the most stable configuration with band gaps typically around 2.13eV [19,20].

The LCCs possess simple phonon structures presenting longitudinal and transversal modes when they are host-free [8]. When encapsulated, however, LCCs share their main axis with their host CNTs and this configuration inhibits transversal modes [20-23]. These phonons possess long mean free paths ($\sim 0.5 - 2.5\mu$m) and lifetimes ($\sim 30 - 110$ps), which highly suppresses phonon-phonon interactions (ph-ph) in LCCs [8] when compared with other carbon materials [24-26]. The optical longitudinal mode (in-axis out-of-phase C-atom vibrations), so-called C-band, with frequencies ω_{LCC} around 1850 cm^{-1}, is an easily trackable Raman spectroscopic signature and due to the weak nature of ph-ph it is an excellent probe to study mechanical and thermal properties [27-32]. The C-band has been characterized in the literature via room-temperature [19,20] and pressure-dependent Raman spectroscopy [21-23] but its use to obtain important mechanical [22] and thermal observables (this work) is a novel concept. Additionally, it is well known that ω_{LCC} is proportional to N^{-1}, where N is the number of carbon atoms [17,22].

Other complex chain-like structures have also been reported [33-39]. Chorro et al. [33], Rols et al. [34], and Cambedouzou et al. [35] showed that C_{60} carbon peapods inserted in SWNTs submitted to various pressure and temperatures could undergo, for example, polymerization (for pressures around 4GPa), high orientational mobility (even for T<100K) and fast diffusional reorientations at T=200K. In another study, Bousige et al. [36], showed evidences of melting and liquid phases for C_{60} chains inside CNTs, revealing that such quasi-1D system behaves as a harmonic crystal for T≤550K (suggesting inefficient ph-ph), transitions to a liquid phase for T≈650K and evolves to a complete disappearance of any structural correlations for T≥850K. All these studies suggest that the interactions between C_{60} molecules and the CNTs' walls are mostly a second order effect. More recently, sulfur chains inside SWNTs have also demonstrated enhanced field-emission properties and outstanding gas-sensing properties [37-39]. In this context, the study of LCCs' thermodynamic properties could greatly benefit other encapsulated 1D systems.

The responses of materials to changing temperatures are closely related to the lattice thermal expansion (LTE) and anharmonic effects [27-32]. The former is associated to electron-phonon couplings (e-ph) and the latter is associated to ph-ph. Usually, ph-ph renormalize phonon energies, playing marginal roles in the understanding of electronic and thermal properties of materials. When it comes to thermal properties, LCCs become particularly interesting and seem to be ahead of other materials such as fullerenes and transition metal dichalcogenides (TMDs) [40-43]. However, detailed studies of e-ph, ph-ph and thermal effects on LCCs inside CNTs are still missing. Recently, theoretical results by Wong et al. reported the LCC's coefficient of thermal expansion (CTE) to be around 7.0×10^{-5} K^{-1} [44], which is much higher than that of CNTs [45], graphene [46], TMDs [47,48] and hexagonal boron nitride [49]. In fact, very little has been explored about LCCs temperature-dependent phenomena, and important works available in the literature are theoretical simulations [4,8,41]. In 2016, Shi et al. studied LCCs inside DWCNT and showed that the C-band linewidth (lifetime) of LCCs increases (decreases) with increasing temperature [1]. They explained their findings in terms of ph-ph and interactions between LCCs and the DWCNTs' inner walls, despite their weak Van der Waals interactions [22,33-35,50-52]. To the best of our knowledge, there is no quantitative temperature-dependent study on ω_{LCC} and its connection to thermodynamic observables.

In this letter, the ω_{LCC} temperature-dependence of distinct LCCs is used as a direct probe to their thermodynamic observables in a wide range of temperatures, showing that fundamental thermodynamic relations follow universal behaviors that only depend on the temperature and number of carbon atoms. Our findings show an unprecedented conclusion: these true one-dimensional systems are well described by the Debye's model even for T at and above 300K, indicating that ph-ph are negligible indeed.

The LCCs encapsulated by multi-walled CNTs (LCC@MWCNTs) were synthesized using arc discharge [19], while the LCCs encapsulated by double-walled CNTs (LCC@DWCNTs) were synthesized using catalyzed chemical vapor deposition [53,54]. The MWCNTs' purity with regard to nanoparticles is ≈80% with average diameters (length) of 10.4nm (2.3mm). The DWCNTs' synthesis yielded over 95% of highly pure and crystalline DWCNTs with an outer diameter of ≈1.6nm. The encapsulated LCCs were then obtained by submitting the DWCNTs to thermal treatment for 30 minutes at 1500$^{\mathrm{o}}$C in a graphite furnace containing high purity argon gas. The LCC@CNTs filling ratio is ≈80% [19,53,54]. The samples were dispersed in acetone and sonicated for 2 hours and then drop-casted onto a Si wafer of ≈1cm^2 area. Raman spectra were acquired with a 50× objective in a backscattering geometry using an Andor iDus 401 series CCD coupled to a Shamrock spectrometer (1200 lines/mm grating; spectral resolution of ≈$\pm$0.5cm^{-1}). Samples were resonantly excited with 532nm (2.33eV) and 632nm (1.96eV) lasers under constant power density of 0.25mW/μm^2.

The correlation between LCC's C-band frequency and N indicates LCCs with 36 to 86 carbon atoms in LCC@MWCNTs and LCCs with 35 to 39 carbon atoms in LCC@DWCNTs [1,7,11,17,21,23,55]. Representative Raman spectra at 300K and C-band spectra fitted with Lorentzian curves are shown in Figures S1(a)-(c), section S1 in the supplementary material (SM) [56]. The MWCNTs host six distinct LCCs and the DWCNTs host four distinct LCCs. For LCC@MWCNTs, each LCC is labelled $\mathrm{LCC}_{\mathrm{i}}^{\mathrm{MW}}$ (i=1, 2, 3, 4, 5 and 6), where i=1 (i=6) represents the longest (shortest) LCC. Their respective room-temperature frequencies are $\omega_{\mathrm{LCC}_1}^{\mathrm{MW}}$ =1796.0cm^{-1}, $\omega_{\mathrm{LCC}_2}^{\mathrm{MW}}$ =1804.0cm^{-1}, $\omega_{\mathrm{LCC}_3}^{\mathrm{MW}}$=1839.0cm^{-1}, $\omega_{\mathrm{LCC}_4}^{\mathrm{MW}}$=1843.0cm^{-1}, $\omega_{\mathrm{LCC}_5}^{\mathrm{MW}}$=1854.0cm^{-1} and $\omega_{\mathrm{LCC}_6}^{\mathrm{MW}}$=1863.0cm^{-1}. Similarly, for the LCC@DWCNTs, each LCC is labelled $\mathrm{LCC}_1^{\mathrm{DW}}$ (longest LCC) and $\mathrm{LCC}_4^{\mathrm{DW}}$ (shortest LCC), whose frequencies are $\omega_{\mathrm{LCC}_1}^{\mathrm{DW}}$=1852.0cm^{-1}, $\omega_{\mathrm{LCC}_2}^{\mathrm{DW}}$=1856.0cm^{-1}, $\omega_{\mathrm{LCC}_3}^{\mathrm{DW}}$ =1860.0cm^{-1}, and $\omega_{\mathrm{LCC}_4}^{\mathrm{DW}}$ =1863.0cm^{-1}. The T-dependence of $\omega_{\mathrm{LCC}_{\mathrm{i}}}^{\mathrm{MW}}$ and $\omega_{\mathrm{LCC}_{\mathrm{i}}}^{\mathrm{DW}}$ shows that $\omega_{\mathrm{LCC}}(\mathrm{T})$=$\omega_{\mathrm{LCC}}^{0} - \left(\frac{\mathrm{d}^2\omega_{\mathrm{LCC}}}{\mathrm{dT}^2}\right)\mathrm{T}^2$, where $\omega_{\mathrm{LCC}}^{0}$ is the frequency at 0K (Figures S2(a)-(c), section S1 in SM). In the absence of ph-ph, $\Delta\omega_{\mathrm{LCC}}(\mathrm{T})$=$\omega_{\mathrm{LCC}}(\mathrm{T}) - \omega_{\mathrm{LCC}}^{0}$ (see Figure 1(a)) will depend mostly on LTE, being directly linked to observables such as specific heat ($\mathrm{c_V}(\mathrm{T})$), coefficient of thermal expansion - CTE ($\alpha(\mathrm{T})$), thermal strain (ε_{T}) and the Grüneisen parameter (γ_{P}) (P=constant pressure).

The literature [20-23,33-36,52] has shown that: **(1)** 1D chains of atoms or molecules are independent of force fields in the CNTs' radial direction [33-36]; **(2)** spectral features from the hosting CNTs and LCCs are independent, even under high pressures [20-23]. The CNTs provide an environment whose force field are sufficient to stabilize the LCCs and inhibit transversal vibrations but not sufficient to entangle CNTs and LCCs properties; and **(3)** interactions between distinct LCCs are not strong enough to affect their structures even at high pressures [20-23]. Therefore, transverse vibrations and mutual interactions between distinct LCCs, and LCCs and CNTs are second order effects. These, together with the absence of ph-ph lead us to hypothesize that: **(1)** LCCs are truly 1D Debye's materials even at T=300K (note that most materials are well described within the Debye's formalism only at very low temperatures (T<<300K) [57,58]); **(2)** any phonon frequency variation with T is connected solely with lattice expansion or contraction; and **(3)** since ph-ph are suppressed, γ_P is T-independent.

The Debye's model does not take into account ph-ph and it is known to work very well for temperatures such that $\frac{T_D}{T} \rightarrow \infty$, where T_D is the Debye's temperature. The Debye's temperature is proportional to the maximum excitable phonon frequency obtained from phonon density of states or dispersion [57,58]. For LCCs, the maximum excitable phonon frequency is set by ω_{LCC}, resulting in $T_D = T_{LCC} = \frac{\hbar\omega_{LCC}}{k_b}$ between 2584K (longest LCC) and 2680K (shortest LCC), where k_b is the Boltzmann constant and $\hbar = \frac{h}{2\pi}$ (h is the Planck's constant). Under the Debye's model formalism (from now on DMF), the canonical partition function for LCCs is given by (section S2 in SM for additional details) [56]:

$$\mathrm{Ln}\, Z = -N \frac{T}{T_{LCC}} \int_0^{\frac{T_{LCC}}{T}} \mathrm{Ln}[1 - \exp(-x)]dx, \qquad (01)$$

where $x = \frac{\hbar\omega_{ph}}{k_b T} = \frac{T_{ph}}{T}$, ω_{ph} is the phonon frequency and T_{ph} is the phonon equivalent temperature. Upon integration by parts, Equation 01 becomes:

$$\ln Z \approx N \frac{T}{T_{LCC}} \int_0^{\frac{T_{LCC}}{T}} \frac{x}{e^x - 1} dx. \qquad (02)$$

For $T << T_{LCC}$, $\frac{T_{LCC}}{T} \rightarrow \infty$ and Equation 02 is simplified to:

$$\mathrm{Ln}\, Z \approx N \frac{T}{T_{LCC}} \int_0^{\infty} \frac{x}{e^x - 1} dx = N \frac{T}{T_{LCC}} \left(\frac{\pi^2}{6}\right) = \frac{N k_b \pi^2}{6\hbar} \frac{T}{\omega_{LCC}(T)}, \qquad (03)$$

where $\int_0^{\infty} \frac{x}{e^x - 1} dx = \frac{\pi^2}{6}$. In our experiments, the temperature variation is not sufficiently large to take LCCs out of the harmonic oscillation regime but it is sufficient to renormalize ω_{LCC} leading to important T-dependent corrections. Therefore, the LCCs' internal energy per N, $u(T)$, $c_v(T)$ and $\alpha(T)$must contain one term representing the Debye's approximation plus corrections involving derivatives of $\omega_{LCC}(T)$. This way $u(T)$ is:

$$u(T) = \frac{k_b T^2}{N} \frac{d(\mathrm{Ln}\, Z)}{dT} = \frac{k_b^2 \pi^2}{6\hbar} \frac{T^2}{\omega_{LCC}(T)} \left[1 - \frac{T}{\omega_{LCC}(T)} \frac{d\omega_{LCC}}{dT}\right], \qquad (04)$$

Figure 1(b) shows that $u(T)$ is size-independent. Equation 04 leads to the heat capacity per N - $c_v(T)$:

$$c_v(T) = \frac{du}{dT} = \frac{(k_b \pi)^2}{3\hbar} \frac{T}{\omega_{LCC}(T)} \left\{1 - 2 \frac{T}{\omega_{LCC}(T)} \frac{d\omega_{LCC}}{dT} + \frac{T^2}{\omega_{LCC}^2(T)} \left[\left(\frac{d\omega_{LCC}}{dT}\right)^2 - \frac{\omega_{LCC}}{2} \frac{d^2\omega_{LCC}}{dT^2}\right]\right\}, \qquad (05)$$

being $\alpha(T)$ given by [56-59]:

$$\alpha(T) = -\frac{\delta}{2\Theta^2}\frac{c_v(T)}{a_{C-C}} = \frac{42(k_b\pi)^2}{3\hbar m a_{c-c}^2}\frac{T}{\omega_{LCC}^3(T)}\left\{1 - 2\frac{T}{\omega_{LCC}(T)}\frac{d\omega_{LCC}}{dT} + \frac{T^2}{\omega_{LCC}^2(T)}\left[\left(\frac{d\omega_{LCC}}{dT}\right)^2 - \frac{\omega_{LCC}}{2}\frac{d^2\omega_{LCC}}{dT^2}\right]\right\}, \quad (06)$$

where a_{c-c}=1.37 Å is the average C-C distance. The parameters $\Theta$and δ are obtained from the second and third derivatives of the series expansion: $U(R) \approx U(a_{c-c}) + \left(\frac{dU}{dR}\right)_{R=a_{c-c}}(R - a_{c-c}) + \frac{1}{2}\left(\frac{d^2U}{dR^2}\right)_{R=a_{c-c}}(R - a_{c-c})^2 + \frac{1}{6}\left(\frac{d^3U}{dR^3}\right)_{R=a_{c-c}}(R - a_{c-c})^3 + \cdots$, where $U(R) = \varepsilon\left[\left(\frac{a_{c-c}}{R}\right)^{12} - 2\left(\frac{a_{c-c}}{R}\right)^6\right]$ is the Lennard-Jones potential (LJ) (R corresponds to the C-atom coordinate and ε is the potential depth). The LJ is chosen based on recent calculations by Wang and Lin [8], whose work describes LCCs' phonon dispersions quite accurately by modeling single and triple carbon bonds using such potential. Therefore, $\left(\frac{dU}{dR}\right)_{R=a_{c-c}} = 0$, $\frac{1}{2}\left(\frac{d^2U}{dR^2}\right)_{R=a_{c-c}} = \frac{1}{2}\left(\frac{72\varepsilon}{a_{c-c}^2}\right)$ and $\frac{1}{6}\left(\frac{d^3U}{dR^3}\right)_{R=a_{c-c}} = \frac{1}{6}\left(-\frac{1512\varepsilon}{a_{c-c}^3}\right)$. The second derivative is associated with the spring-mass harmonic potential. This means that: $\Theta = \frac{1}{2}\frac{d^2U}{dR^2} = \frac{m[\omega_{LCC}(T)]^2}{2}$, $\delta = -\frac{21m[\omega_{LCC}(T)]^2}{a_{c-c}}$ and $\varepsilon = \frac{mR_m^2\left(\omega_{LCC}^0\right)^2}{72}$. With $\omega_{LCC}(T)$ and $\frac{d\omega_{LCC}}{dT}=-2\left(\frac{d^2\omega_{LCC}}{dT^2}\right)T$ we calculate $u(T)$, $c_v(T)$, $\alpha(T)$ and $\varepsilon(T)$ for each LCC.

The experimental $\alpha(T)$ (Figure 1(c)) and $c_v(T)$ (Figure 1(d)) endorse that LCCs are well described under DMF. Multi-Walled CNTs [60], graphene [46], bi-layer graphene [46] and graphite [61] (quasi-one, two- and three-dimensional sp^2 materials, respectively) present negative $\alpha(T)$ and ph-ph are fundamental to understand their $\Delta\omega(T)$ even for the temperatures in the range 0K≤T≤300K. Here, we see that for LCCs (sp materials) these dependencies are modified: $\alpha(T)$ is always positive and linearly dependent on T with a value of 5.0 x $10^{-5}K^{-1}$ (4.5 x $10^{-5}K^{-1}$) at 300K for the longest (shortest) chains, which is close to those reported for SWCNTs ($\alpha(T)$=2 x $10^{-5}K^{-1}$ at 300K) [62] and 10x higher in magnitude than the value reported for graphene ($\alpha(T)$=-8.1 x $10^{-6}K^{-1}$ at 300K) [46]. These values are in remarkably good agreement with the theoretical prediction of 7 x $10^{-5}K^{-1}$by Wong et al. [44]. To the best of our knowledge, we present the first experimental evaluation of the LCCs' $c_v(T)$, which shows a unified linear dependence with T. The value 0.25J/gK found at 300K are close to those for Graphite (0.7J/gK) and Graphene (0.5J/gK) [63,64]. We note that 0.25J/gK is 4.6 times smaller than the value 1.16J/gK predicted by Zhang et al. [4], who performed first-principles calculations for very short LCCs having a (5, 5) carbon nanotube as reference (non-negligible boundary conditions), what could explain such discrepancy.

The heat extracted from the LCCs leads to their shrinkage, which changes the LCCs' T-dependent internal pressure. This internal pressure is associated with both the system's entropy and thermal strain (ε_T). The thermal strain possesses a T^2 dependence (Figure 1(e)) in perfect analogy with the P^2 dependence obeserved by Sharma et al. [22]. Therefore, in terms of behaviors, strains caused by either T or P differ only in magnitude. In Figure 1(f), ε_T is plotted against $\Delta\omega_{LCC}(T)$. The graphic shows the linear behavior expected for small magnitude strains [22,57,58], which allow us to conclude that, for a given ε_T, larger LCCs experience larger $\Delta\omega_{LCC}(T)$, in further agreement with Sharma et al. [22].

For negligible ph-ph, $\Delta\omega(T)$ should be fully described in terms of the LTE as:

$$\Delta\omega_{LTE}(T) = \omega_{LCC}^0\left(e^{-\gamma_P\int d\varepsilon} - 1\right), \quad (07)$$

where $d\varepsilon=\alpha(T)dT$ is the thermal strain between T and $T+dT$. Therefore, if our hypotheses are correct, by using the observables described in Equations 04 through 06, Equation 07 should be equivalent to the obtained empirical relation $\Delta\omega_{LCC}(T)=-\left(\frac{d^2\omega_{LCC}}{dT^2}\right)T^2$ using γ_P as a fitting parameter. In the quasi-harmonic regime there is no distinction between γ_P and γ_T (Grüneisen parameter at constant T), i.e., $\Delta\gamma\approx0$ [65]. As shown in Figure 01(a), Equation 07 fits the experimental $\Delta\omega_{LCC}(T)$ with γ_P ranging from 0.42 (shortest LCC) to 0.79 (longest LCC). These values agree with γ_T found in our previous work [22], which confirms that $\Delta\gamma\approx0$ and endorses the absence of ph-ph. Note that Sharma et al. [22] also showed that smaller LCCs present smaller γ_T in the quasi-harmonic regime.

The absence of ph-ph, the successful description of LCCs' properties within DMF for $T\leq300K$, and the T-independent values of γ_P indicate that the corrections proposed are valid as long as the Debye's temperature T_{LCC} is much larger than an upper limit (T_{max}) after which the approximation $\frac{T_{LCC}}{T}\rightarrow\infty$ is no longer valid. Inspection of Equation 02 shows that the $\ln Z$ behavior is determined by the integrand $\frac{x}{e^x-1}$, which is most relevant for x between 0 and 4, as seen in Figure 2(a). This way T_{max} is determined such that $\frac{T_{LCC}}{T_{max}}=4$, which means that $T_{max}=\frac{T_{LCC}}{4}\approx700K$. For $T\leq300K$ the correction terms are negligible for every observable but for 300K<T<700K (see insets in Figure 1), the corrections become increasingly important. Our model predicts that $\Delta\omega_{LCC}(T)$ decreases at a slower rate with changing T (inset in Figure 1(a)), while $\alpha(T)$ and $c_v(T)$ increase at a slower rate in comparison with the pure Debye's model (insets in Figures 1(c) and (d), respectively). The magnitude of the corrections depends on $\frac{d^2\omega_{LCC}}{dT^2}$ and, consequently, on N (Figure 2(b)): the bigger the N the larger the correction. This is expected since the LCCs' thermal properties are connected to the intrinsic character of both single and triple bonds, which assume effective values reflecting the size of each LCC until the thermodynamic limit is reached (see section S3 in SM for additional details [56]).

As shown in Figure 2(b), both γ_P and $\frac{d^2\omega_{LCC}}{dT^2}$ display universal dependences on N given by $\gamma_P(N)=\ln(N-20)^{0.18}$ and $\frac{d^2\omega_{LCC}}{dT^2}=A+\frac{B}{N}$ (A =-1.63 x 10^{-4} cm^{-1}K^{-2} and B =35 x 10^{-4} cm^{-1}K^{-2}), respectively. The $\frac{d^2\omega_{LCC}}{dT^2}$ relation with N lead us to the $\omega_{LCC}(N,T)$ universal relation:

$$\omega_{LCC}(N,T)=\omega^0_{LCC}(N,0)-\left(A+\frac{B}{N}\right)T^2, \qquad (08)$$

where $\omega^0_{LCC}(N,0)=\left(1757+\frac{3980}{N}\right)$cm^{-1} [17], see Figure 2(c). The results for $\Delta\omega_{LCC}(T)$ also show that the LCCs' hosts do not influence the LCC's responses to T (Figure S5 in SM [56]). The differences in the values observed for $\alpha(T)$, $c_v(T)$ and $\Delta\omega_{LCC}(T)$ comparing the solid (pure Debye's model) and the dashed curves (pure Debye's model + corrections) in Figures 1(a)-(d) allowed us to rewrite Equations 05, 06 and 07 in terms of N and T. Such description is advantageous since it is now possible to predict the thermal properties of any chain at any $0K\leq T\leq700K$:

$$\alpha(N,T)=985\frac{T}{\omega^3_{LCC}(N,T)}-(3.22\times10^{-10})\sqrt{(T-300)^3(N-20)}, \qquad (09)$$

$$c_v(N,T)=(1.6\times10^{-3})\omega^2_{LCC}(N,T)\alpha(N,T), \qquad (10)$$

where $\omega_{\mathrm{LCC}}(\mathrm{N},\mathrm{T})$ is given by Equation 08. Equations 09 and 10 allow for the determination of $\varepsilon_{\mathrm{T}}(\mathrm{N},\mathrm{T}) = \int \alpha(\mathrm{N},\mathrm{T})\mathrm{dT}$ and $\mathrm{u}(\mathrm{N},\mathrm{T}) = \int \mathrm{c_v}(\mathrm{N},\mathrm{T})\mathrm{dT}$. Finally, $\Delta\omega_{\mathrm{LCC}}(\mathrm{N},\mathrm{T}) = -\left(\frac{\mathrm{d}^2\omega_{\mathrm{LCC}}}{\mathrm{dT}^2}\right)\mathrm{T}^2 + \Delta(\mathrm{N},\mathrm{T})$, which gives:

$$\Delta\omega_{\mathrm{LCC}}(\mathrm{N},\mathrm{T}) = -\left(\mathrm{A} + \frac{\mathrm{B}}{\mathrm{N}}\right)\mathrm{T}^2 + (5.24 \times 10^{-7})(\mathrm{T} - 300)^2(\mathrm{N} - 20), \qquad (11)$$

where $\Delta(\mathrm{N},\mathrm{T})= \Delta\omega_{\mathrm{LCC}}^{\mathrm{Corr.}} - \Delta\omega_{\mathrm{LCC}}^{\mathrm{Debye}}$ is the difference between $\Delta\omega_{\mathrm{LCC}}^{\mathrm{Corr.}}$ (dashed lines in Figure 1(a)) and $\Delta\omega_{\mathrm{LCC}}^{\mathrm{Debye}}$ (solid lines in Figure 1(a)). The inset in Figure 2(c) shows the representative case for $\Delta(\mathrm{N},700)$.

In summary, the manuscript focuses on the thermodynamic observables associated with LCCs and shows that due to negligible ph-ph, ω_{LCC} acts as a direct probe to the LCCs' thermal properties. Most materials are well described within DMF only at very low temperatures but our results show that LCCs are well explained by DMF even at room temperature and likely for temperatures as high as 700K. By observing the temperature-dependence of $\Delta\omega_{\mathrm{LCC}}(\mathrm{T})$, the thermodynamics associated to LCCs is successfully discussed, showing that fundamental relations such as internal energy, specific heat, coefficient of thermal expansion and thermal strain present (N,T)-dependent universal behaviors. We present a simple semi-empirical approach that is in excellent agreement with theoretical results in the literature and useful to other 1D systems.

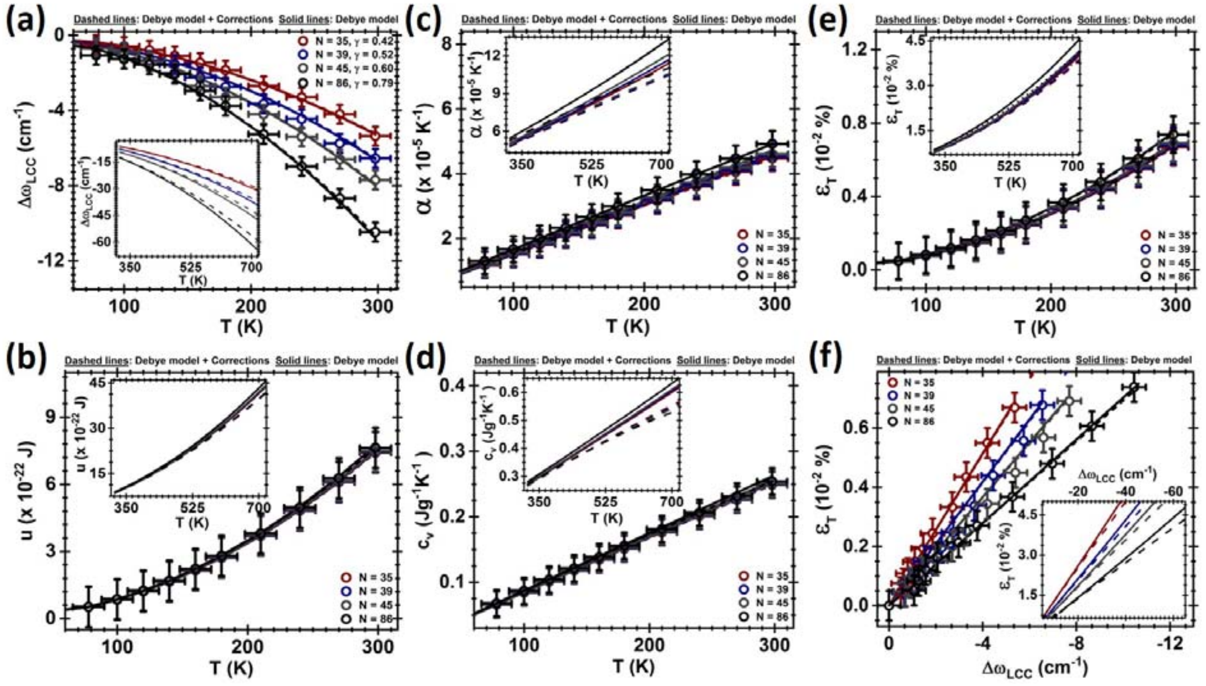

Figure 1: Representative experimental results for LCCs (N=35, N=39, N=45 and N=86): (a) experimental $\Delta\omega_{\mathrm{LCC}}(\mathrm{T})$ evolution with T; (b) the energy per N, $\mathrm{u}(\mathrm{T})$, presents a quadratic, universal and unified behavior with T; (c) $\alpha(\mathrm{T})$ shows a linear universal behavior with T, where LCCs with N from 35 to 45 atoms present very similar $\alpha(\mathrm{T})$. For N=86, however, which is closer to the thermodynamic limit, $\alpha(\mathrm{T})$ increases at a slightly higher rate with increasing T; (d) the heat capacity per N, $\mathrm{c_v}(\mathrm{T})$, presents a linear, universal and unified behavior with T; (e) A T^2 universal dependence is observed for the thermal strain $\varepsilon_{\mathrm{T}}(\mathrm{T})$ with N from 35 to 45 atoms presenting very similar $\varepsilon_{\mathrm{T}}(\mathrm{T})$, while for N=86 $\varepsilon_{\mathrm{T}}(\mathrm{T})$ increases at a slightly higher rate with increasing T; (f) Every LCC presents a distinct linear dependence of ε_{T} with $\Delta\omega_{\mathrm{LCC}}(\mathrm{T})$. The curves show the predictions of the pure Debye's model (solid lines) compared with the model proposed (dashed lines) and the insets in (a)-(f) suggest that for temperatures 300K≤T≤700K the observables evolve more slowly with increasing T. Figures S3 and S4 in SM show the results including all the 10 LCCs measured in this work.

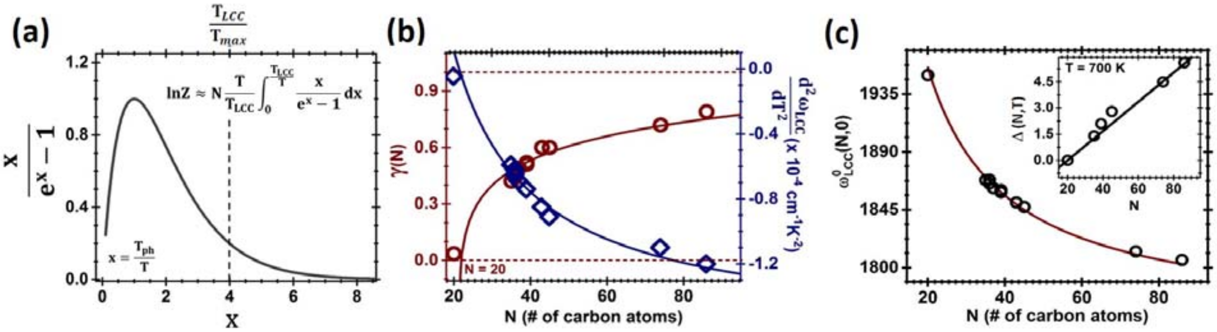

Figure 2: (a) the distribution function $\frac{x}{e^x-1}$ with $x = \frac{T_{ph}}{T}$ is fundamental to identify the high temperature limit (T_{max}) of the model. The distribution is most relevant for 0≤x≤4, which implies that $T_{max} = \frac{T_{LCC}}{4} \approx$ 700K (see inset). (b) Universal dependences with N for both $\gamma_P(N)$=$\ln(N -$ 200.18 (wine solid lines) and $d2\omega LCCdT2$ =$A+BN$ (navy solid line with A =-1.63 x 10^{-4} $cm^{-1}K^{-2}$ and B =35 x 10^{-4} $cm^{-1}K^{-2}$). The symbols (wine circles and navy diamonds for γ_P and $\frac{d^2\omega_{LCC}}{dT^2}$, respectively) represent the experimental data. (c) $\omega^0_{LCC}(N,0)$=$\left(1757 + \frac{3980}{N}\right)$$cm^{-1}$, where $\omega^0_{LCC}(N,0)$ is the C-band frequency at T=0K. The open circles represent the experimental data. The inset shows a representative case at T=700K for $\Delta(N,T)$= $\Delta\omega^{Corr.}_{LCC} - \Delta\omega^{Debye}_{LCC}$, which shows how the difference between $\Delta\omega^{Corr.}_{LCC}$ proposed here (dashed lines in Figure 1(a)) and $\Delta\omega^{Debye}_{LCC}$ (solid lines in Figure 1(a)) progresses with N.

Acknowledgements

This material is based upon work supported by the National Science Foundation under Grant No. [1848418]. PTA, KS, NMBN, NLC and ARP acknowledge both the American Physical Society (APS) and the Brazilian Physical Society (SBF – Portuguese acronym) for supporting this research through the Brazil-US PhD Exchange program. YAK acknowledges financial support from a National Research Foundation of Korea (NRF) grant funded by the Korea government (MSIP) (No. 2017M3A7B4014045). ARP would like to thank UFC CAPES-PrInt research proposal for the financial support in the scopes of 01/2018 and 41/2017 public calls from UFC and CAPES, respectively.

References

[1] L. Shi, P. Rohringer, K. Suenaga, Y. Niimi, J. Kotakoski, J. C. Meyer, H. Peterlik, M. Wanko, S. Cahangirov, A. Rubio, Z. J. Lapin, L. Novotny, P. Ayala, and T. Pichler, Confined linear carbon chains as a route to bulk carbyne, Nat. Mater. 15, 634-639 (2016).
[2] A. Hirsch, The era of carbon allotropes, Nat. Mater. 9, 868 (2010).
[3] X. Zhao, Y. Ando, Y. Liu, M. Jinno, and T. Suzuki, Carbon nanowire made of a long linear carbon chain inserted inside a multiwalled carbon nanotube, Phys. Rev. Lett. 90, 187401 (2003).
[4] Y. Zhang, Y. Su, L. Wang, E. S. Kong, X. Chen, and Y. Zhang, A one-dimensional extremely covalent material: monatomic carbon linear chain, Nanoscale Res. Lett. 6, 577 (2011).
[5] C. Zhao, R. Kitaura, H. Hara, S. Irle, and H. Shinohara, Growth of Linear Carbon Chains inside Thin Double-Wall Carbon Nanotubes, J. Phys. Chem. C 115, 13166-13170 (2011).
[6] P. Smith and P. R. Buseck, Carbyne forms of carbon: do they exist?, Science 216, 984-986 (1982).
[7] A. K. Nair, S. W. Cranford, and M. J. Buehler, The minimal nanowire: Mechanical properties of carbyne, EPL (Europhysics Letters) 95, 16002 (2011).
[8] M. Wang and S. Lin, Ballistic Thermal Transport in Carbyne and Cumulene with Micron-Scale Spectral Acoustic Phonon Mean Free Path, Sci. Rep. 5, 18122 (2015).
[9] Z. Wang, X. Ke, Z. Zhu, F. Zhang, M. Ruan, and J. Yang, Carbon-atom chain formation in the core of nanotubes, Phys. Rev. B 61, R2472 (2000).
[10] L. Moura, L. Malard, M. Carneiro, P. Venezuela, R. B. Capaz, D. Nishide, Y. Achiba, H. Shinohara, and M. Pimenta, Charge transfer and screening effects in polyynes encapsulated inside single-wall carbon nanotubes, Phys. Rev. B 80, 161401 (2009).
[11] L. Shi, P. Rohringer, M. Wanko, A. Rubio, S. Waßerroth, S. Reich, S. Cambré, W. Wenseleers, P. Ayala, and T. Pichler, Electronic band gaps of confined linear carbon chains ranging from polyyne to carbyne, Phys. Rev. Mater. 1 (2017).
[12] O. Cretu, A. R. Botello-Mendez, I. Janowska, C. Pham-Huu, J.-C. Charlier, and F. Banhart, Electrical transport measured in atomic carbon chains, Nano Lett. 13, 3487-3493 (2013).
[13] N. Lang and P. Avouris, Oscillatory conductance of carbon-atom wires, Phys. Rev. Lett. 81, 3515 (1998).
[14] R. J. Lagow, J. J. Kampa, H.-C. Wei, S. L. Battle, J. W. Genge, D. A. Laude, C. J. Harper, R. Bau, R. C. Stevens, and J. F. Haw, Synthesis of linear acetylenic carbon: the" sp" carbon allotrope, Science 267, 362-367 (1995).
[15] D. Nishide, H. Dohi, T. Wakabayashi, E. Nishibori, S. Aoyagi, M. Ishida, S. Kikuchi, R. Kitaura, T. Sugai, and M. Sakata, Single-wall carbon nanotubes encaging linear chain C10H2 polyyne molecules inside, Chem. Phys. Lett. 428, 356-360 (2006).
[16] F. Cataldo, Polyynes: synthesis, properties, and applications, (CRC Press, Boca Raton, 2005).

[17] J. Kastner, H. Kuzmany, L. Kavan, F. Dousek, and J. Kürti, Reductive preparation of carbyne with high yield. An in situ Raman scattering study, Macromolecules 28, 344-353 (1995).

[18] F. Diederich and M. Kivala, All-carbon scaffolds by rational design, Adv. Mater. 22, 803-812 (2010).

[19] C. S. Kang, K. Fujisawa, Y. I. Ko, H. Muramatsu, T. Hayashi, M. Endo, H. J. Kim, D. Lim, J. H. Kim, and Y. C. Jung, Linear carbon chains inside multi-walled carbon nanotubes: growth mechanism, thermal stability and electrical properties, Carbon 107, 217-224 (2016).

[20] N. Andrade, T. Vasconcelos, C. Gouvea, B. Archanjo, C. Achete, Y. Kim, M. Endo, C. Fantini, M. Dresselhaus, and A. Souza Filho, Linear carbon chains encapsulated in multiwall carbon nanotubes: Resonance Raman spectroscopy and transmission electron microscopy studies, Carbon 90, 172-180 (2015).

[21] N. F. Andrade, A. L. Aguiar, Y. A. Kim, M. Endo, P. T. C. Freire, G. Brunetto, D. S. Galvão, M. S. Dresselhaus, and A. G. Souza Filho, Linear Carbon Chains under High-Pressure Conditions, J. Phys. Chem. C 119, 10669-10676 (2015).

[22] K. Sharma, N. L. Costa, Y. A. Kim, H. Muramatsu, N. M. B. Neto, L. G. Martins, J. Kong, A. R. Paschoal, and P. T. Araujo, Anharmonicity and Universal Response of Linear Carbon Chain Mechanical Properties under Hydrostatic Pressure, Phys. Rev. Lett. 125, 105501 (2020).

[23] W. Q. Neves, R. S. Alencar, R. S. Ferreira, A. C. Torres-Dias, N. F. Andrade, A. San-Miguel, Y. A. Kim, M. Endo, D. W. Kim, H. Muramatsu, A. L. Aguiar, and A. G. Souza Filho, Effects of pressure on the structural and electronic properties of linear carbon chains encapsulated in double wall carbon nanotubes, Carbon 133, 446-456 (2018).

[24] K. Kang, D. Abdula, D. G. Cahill, and M. Shim, Lifetimes of optical phonons in graphene and graphite by time-resolved incoherent anti-Stokes Raman scattering, Phys. Rev. B 81, 165405 (2010).

[25] S. Kutrovskaya, A. Osipov, S. Baryshev, A. Zasedatelev, V. Samyshkin, S. Demirchyan, O. Pulci, D. Grassano, L. Gontrani, and R. R. Hartmann, Excitonic fine structure in emission of linear carbon chains, Nano Lett. 20, 6502-6509 (2020).

[26] N. Z. Swinteck, K. Muralidharan, and P. A. Deymier, Phonon scattering in one-dimensional anharmonic crystals and superlattices: Analytical and numerical study, Journal of vibration and acoustics 135 (2013).

[27] K. Gao, R. Dai, Z. Zhang, and Z. Ding, Anharmonic effects in single-walled carbon nanotubes, Journal of Physics: Condensed Matter 19, 486210 (2007).

[28] W. Li, Z. Shen, Z. Feng, and S. Chua, Temperature dependence of Raman scattering in hexagonal gallium nitride films, J. Appl. Phys. 87, 3332-3337 (2000).

[29] X. Huang, Y. Gao, T. Yang, W. Ren, H.-M. Cheng, and T. Lai, Quantitative Analysis of Temperature Dependence of Raman shift of monolayer WS 2, Sci. Rep. 6, 32236 (2016).

[30] P. Klemens, Anharmonic decay of optical phonons, Phys. Rev. 148, 845 (1966).

[31] P. T. Araujo, Anharmonicities in phonon combinations and overtones in bilayered graphene: A temperature-dependent approach, Phys. Rev. B 97, 205441 (2018).

[32] M. Balkanski, R. Wallis, and E. Haro, Anharmonic effects in light scattering due to optical phonons in silicon, Phys. Rev. B 28, 1928 (1983).

[33] M. Chorro, S. Rols, J. Cambedouzou, L. Alvarez, R. Almairac, J.-L. Sauvajol, J.-L. Hodeau, L. Marques, M. Mezouar, and H. Kataura, Structural properties of carbon peapods under extreme conditions studied using in situ x-ray diffraction, Phys. Rev. B 74, 205425 (2006).

[34] S. Rols, J. Cambedouzou, M. Chorro, H. Schober, V. Agafonov, P. Launois, V. Davydov, A. Rakhmanina, H. Kataura, and J.-L. Sauvajol, How confinement affects the dynamics of C 60 in carbon nanopeapods, Phys. Rev. Lett. 101, 065507 (2008).

[35] J. Cambedouzou, S. Rols, R. Almairac, J.-L. Sauvajol, H. Kataura, and H. Schober, Low-frequency excitations of C 60 chains inserted inside single-walled carbon nanotubes, Phys. Rev. B 71, 041403 (2005).

[36] C. Bousige, S. Rols, J. Ollivier, H. Schober, P. Fouquet, G. G. Simeoni, V. Agafonov, V. Davydov, Y. Niimi, and K. Suenaga, From a one-dimensional crystal to a one-dimensional liquid: A comprehensive dynamical study of C 60 peapods, Phys. Rev. B 87, 195438 (2013).
[37] J. Yang, J. Lee, J. Lee, and W. Yi, Field-emission properties of sulfur chain-encapsulated single-walled carbon nanotubes, Diam. Relat. Mater. 101, 107554 (2020).
[38] J. Yang, J. Lee, J. Lee, and W. Yi, Gas sensing mechanism of sulfur chain-encapsulated single-walled carbon nanotubes, Diam. Relat. Mater. 97, 107474 (2019).
[39] T. Fujimori, A. Morelos-Gomez, Z. Zhu, H. Muramatsu, R. Futamura, K. Urita, M. Terrones, T. Hayashi, M. Endo, S. Y. Hong, Y. C. Choi, D. Tomanek, and K. Kaneko, Conducting linear chains of sulphur inside carbon nanotubes, Nat. Commun. 4, 2162 (2013).
[40] J. Olson, K. Topp, and R. Pohl, Specific heat and thermal conductivity of solid fullerenes, Science 259, 1145-1148 (1993).
[41] Y. Deng and S. W. Cranford, Thermal conductivity of 1D carbyne chains, Computational Materials Science 129, 226-230 (2017).
[42] R. Yan, J. R. Simpson, S. Bertolazzi, J. Brivio, M. Watson, X. Wu, A. Kis, T. Luo, A. R. Hight Walker, and H. G. Xing, Thermal conductivity of monolayer molybdenum disulfide obtained from temperature-dependent Raman spectroscopy, ACS Nano 8, 986-993 (2014).
[43] X. Wang, C. D. Liman, N. D. Treat, M. L. Chabinyc, and D. G. Cahill, Ultralow thermal conductivity of fullerene derivatives, Phys. Rev. B 88, 075310 (2013).
[44] C. Wong, E. Buntov, V. Rychkov, M. Guseva, and A. Zatsepin, Simulation of chemical bond distributions and phase transformation in carbon chains, Carbon 114, 106-110 (2017).
[45] J. Hone, M. Whitney, C. Piskoti, and A. Zettl, Thermal conductivity of single-walled carbon nanotubes, Phys. Rev. B 59, R2514 (1999).
[46] D. Yoon, Y. W. Son, and H. Cheong, Negative thermal expansion coefficient of graphene measured by Raman spectroscopy, Nano Lett. 11, 3227-3231 (2011).
[47] W. Choi, N. Choudhary, G. H. Han, J. Park, D. Akinwande, and Y. H. Lee, Recent development of two-dimensional transition metal dichalcogenides and their applications, Materials Today 20, 116-130 (2017).
[48] C. Muratore, V. Varshney, J. J. Gengler, J. Hu, J. E. Bultman, T. M. Smith, P. J. Shamberger, B. Qiu, X. Ruan, and A. K. Roy, Cross-plane thermal properties of transition metal dichalcogenides, Appl. Phys. Lett. 102, 081604 (2013).
[49] I. Jo, M. T. Pettes, J. Kim, K. Watanabe, T. Taniguchi, Z. Yao, and L. Shi, Thermal conductivity and phonon transport in suspended few-layer hexagonal boron nitride, Nano Lett. 13, 550-554 (2013).
[50] R. Alencar, A. Aguiar, A. Paschoal, P. Freire, Y. Kim, H. Muramatsu, M. Endo, H. Terrones, M. Terrones, and A. San-Miguel, Pressure-induced selectivity for probing inner tubes in double-and triple-walled carbon nanotubes: A resonance raman study, J. Phys. Chem. C 118, 8153-8158 (2014).
[51] J. Arvanitidis, D. Christofilos, K. Papagelis, K. Andrikopoulos, T. Takenobu, Y. Iwasa, H. Kataura, S. Ves, and G. Kourouklis, Pressure screening in the interior of primary shells in double-wall carbon nanotubes, Phys. Rev. B 71, 125404 (2005).
[52] K. Matsuda, Y. Maniwa, and H. Kataura, Highly rotational C 60 dynamics inside single-walled carbon nanotubes: NMR observations, Phys. Rev. B 77, 075421 (2008).
[53] L. Shi, L. Sheng, L. Yu, K. An, Y. Ando, and X. Zhao, Ultra-thin double-walled carbon nanotubes: a novel nanocontainer for preparing atomic wires, Nano Res. 4, 759-766 (2011).
[54] M. Endo, Y. A. Kim, T. Hayashi, H. Muramatsu, M. Terrones, R. Saito, F. Villalpando-Paez, S. G. Chou, and M. S. Dresselhaus, Nanotube Coalescence-Inducing Mode: A Novel Vibrational Mode in Carbon Systems, Small 2, 1031-1036 (2006).
[55] R. S. Alencar, W. Cui, A. C. Torres-Dias, T. F. T. Cerqueira, S. Botti, M. A. L. Marques, O. P. Ferreira, C. Laurent, A. Weibel, D. Machon, D. J. Dunstan, A. G. Souza Filho, and A. San-Miguel, Pressure-induced radial collapse in few-wall carbon nanotubes: A combined theoretical and experimental study, Carbon 125, 429-436 (2017).

[56] See Supplementary Material at (link). The supplementary material brings comprehensive discussions on the theoretical model and experimental methods. It also brings additional figures and a table that contribute with the understanding of the work, which includes Ref. [].

[57] C. Kittel, Introduction to Solid State Physics, (Wiley, New York, 1976), 8th edn., pp. 105-129.

[58] N. W. Ashcroft and N. D. Mermin, Solid State Physics, (Saunders College, Philadelphia, 1976), pp. 451-468.

[59] K. Pathak and B. Deo, Thermal Expansion of a Linear Lattice, physica status solidi (b) 17, 77-81 (1966).

[60] K. Shirasu, G. Yamamoto, I. Tamaki, T. Ogasawara, Y. Shimamura, Y. Inoue, and T. Hashida, Negative axial thermal expansion coefficient of carbon nanotubes: Experimental determination based on measurements of coefficient of thermal expansion for aligned carbon nanotube reinforced epoxy composites, Carbon 95, 904-909 (2015).

[61] D. Tsang, B. Marsden, S. Fok, and G. Hall, Graphite thermal expansion relationship for different temperature ranges, Carbon 43, 2902-2906 (2005).

[62] L. Deng, R. J. Young, I. A. Kinloch, R. Sun, G. Zhang, L. Noé, and M. Monthioux, Coefficient of thermal expansion of carbon nanotubes measured by Raman spectroscopy, Appl. Phys. Lett. 104, 051907 (2014).

[63] E. Pop, V. Varshney, and A. K. Roy, Thermal properties of graphene: Fundamentals and applications, MRS bulletin 37, 1273-1281 (2012).

[64] F. Ma, H. Zheng, Y. Sun, D. Yang, K. Xu, and P. K. Chu, Strain effect on lattice vibration, heat capacity, and thermal conductivity of graphene, Appl. Phys. Lett. 101, 111904 (2012).

[65] G. Lucazeau, Effect of pressure and temperature on Raman spectra of solids: anharmonicity, Journal of Raman Spectroscopy 34, 478-496 (2003).